ADVANCED OPTICAL MATERIALS
www.advopticalmat.de

High-Accuracy Photoplethysmography Array Using Near-Infrared Organic Photodiodes with Ultralow Dark Current

*Giulio Simone, Daniel Tordera, Ezequiel Delvitto, Bart Peeters, Albert J. J. M. van Breemen, Stefan C. J. Meskers, René A. J. Janssen, and Gerwin H. Gelinck**

Reflectance oximeters based on organic photodiode (OPD) arrays offer the potential to map blood pulsation and oxygenation via photoplethysmography (PPG) over a large area and beyond the traditional sensing locations. Here, an organic reflectance PPG array based on 16 × 16 OPD pixels is developed. The individual pixels exhibit near-infrared sensitivity up to ≈950 nm and low dark current density in the order of 10^{-6} mA cm^{-2}. This results in high-quality PPG signals. Analysis of the full PPG waveform yields insight on the artery stiffness and the quality of blood circulation, demonstrating the potential of these arrays beyond pulse oximetry and heart-rate calculation.

Pulse oximeters are noninvasive medical sensors that monitor heartbeat via photoplethysmography (PPG), a widely used optical technique to detect volume changes in the subcutaneous tissue caused by blood pulses. PPG has been used for a wide range of clinical applications, including measuring blood pressure and cardiac output,[1] monitoring respiratory rate[2,3] and depth of anesthesia,[4] assessing arterial blood oxygenation,[5] and detecting peripheral vascular disease.[6] PPG signals are typically acquired by illuminating the skin with light-emitting diodes (LEDs) and detecting light transmitted or reflected by the tissue with a photodiode. Peripheral blood oxygenation (SpO_2) can be assessed by using LEDs that sequentially emit light with different wavelengths, typically in the red and near-infrared (NIR) spectral region, to estimate the ratio of oxyhemoglobin and deoxyhemoglobin in arterial blood. Transmission pulse oximeters restrict the sensing location to tissues that can be transilluminated, generally fingertips or ear lobes. To overcome this limitation, pulse oximeters should be used in reflective mode,[7] that is, sensing light that slightly penetrates in the tissue and is then reflected. This opens the possibility to monitor pulse rate and blood oxygenation beyond the traditional sensing locations (e.g., fingertip and earlob).

Recent developments in the field of organic electronics have led to reflectance oximeters based on organic photodiodes (OPDs).[8–11] The potential for large-area manufacturing using industrially scalable coating techniques,[12] combined with the wide absorption spectrum and high color selectivity,[13] makes OPDs attractive for this class of optoelectronic sensors. Organic reflectance oximeters on light-weight flexible substrates[14] can easily adapt to complex shapes of the body, thereby potentially providing a versatile alternative to rigid conventional designs. Furthermore, the signal-to-noise ratio (SNR) of flexible oximeters is enhanced by the formation of a conformal sensor–skin interface with lower effective impedance,[15–17] which reduces the electronic noise during PPG acquisition. Lochner et al.[8] first combined organic light emitting diodes (OLEDs) with two OPD pixels in an all-organic pulse oximeter. This sensor successfully measured pulse rate and blood oxygenation level within an experimental error of 1% and 2%, respectively. In 2018, Khan et al.[9] presented a reflectance oximeter array composed of four red and four NIR OLEDs, and eight OPDs. Such configuration introduces the functionality of 2D oxygenation mapping capability. The sensor was used to measure oxygen saturation on the forehead with 1.1% error and to create 2D oxygenation maps of adult forearms under under normal and ischemic conditions.

Here, we develop an NIR sensitive OPD array of 16 × 16 pixels and demonstrate its potential in reflectance PPG. Each OPD pixel exhibits NIR sensitivity up to ≈ 950 nm together with a low dark current density in the order of 10^{-6} mA cm^{-2}. As the OPD array is operated in reflective mode, a thin semi-transparent top electrode in each pixel is needed not to hinder light that reaches the fingertip and is then reflected. At the same time, the top electrode must form a continuous layer to ensure low series resistance. To fulfill both requirements, we use a 10 nm Ag top electrode. Notably, we use opaque bottom electrodes in combination with the semi-transparent non-patterned top electrode, so that only reflected light is detected by the OPD array.

Dr. G. Simone, Dr. S. C. J. Meskers, Prof. R. A. J. Janssen, Prof. G. H. Gelinck
Molecular Materials and Nanosystems
Institute of Complex Molecular Systems
Eindhoven University of Technology
P.O. Box 513, Eindhoven 5600 MB, The Netherlands
E-mail: g.h.gelinck@tue.nl
Dr. D. Tordera, E. Delvitto, B. Peeters, Dr. A. J. J. M. van Breemen, Prof. G. H. Gelinck
Holst Centre
TNO-The Dutch Organization for Applied Scientific Research
High Tech Campus 31, Eindhoven 5656 AE, The Netherlands
Prof. R. A. J. Janssen
Dutch Institute for Fundamental Energy Research
De Zaale 20, Eindhoven 5612 AJ, The Netherlands
The ORCID identification number(s) for the author(s) of this article can be found under https://doi.org/10.1002/adom.201901989.

DOI: 10.1002/adom.201901989

Table 1. Comparison between reported organic oximeter arrays based on number (n) of OPD pixels, total area of the sensor, resolution, dark current density (J_d), maximum EQE, and maximum absorption wavelength (λ_{max}).

Reference	n OPD pixels	Area sensor [cm^2]	Resolution [ppi]	J_d [mA cm^{-2}][a)]	EQE$_{max}$[b)] [nm]	λ_{max} [nm]
[8]	2	0.4	6.3	10^{-6} (–2 V)	0.47 (626 nm)	770
[9]	8	18.5	3.3	10^{-6} (–0.5 V)	0.35 (700 nm)	890
[17]	64 500	1.6	508	10^{-4} (–2 V)	1.0 (850 nm)	1000
This work	256	4.0	20.3	8.5×10^{-6} (–3 V)	0.10 (900 nm)	950

[a)]J_d is measured under the applied bias indicated between brackets; [b)]EQE$_{max}$ is measured at the wavelength indicated between brackets.

Our array enables PPG imaging over an area of 1.8 × 2.2 cm with a resolution of 20.3 pixels per inch (ppi). **Table 1** shows a comparison between our organic oximeter array and previously reported work. The comparison is based on number (n) of OPD pixels, total area of the sensor, resolution, dark current density (J_d), maximum external quantum efficiency (EQE$_{max}$), and maximum absorption wavelength (λ_{max}). Each parameter is subject of further discussion in the text.

We establish that the array photoresponse is linear with light intensity within the range used for PPG imaging in this work. Furthermore, we show the uniformity of the photoresponse over the whole pixel array, with negligible pixel-to-pixel variations in photocurrent under the same lighting conditions. This opens the possibility to map the PPG signal over larger area compared to previously reported reflectance oximeter arrays.[9] The quality of the PPG signal can be increased when post-processing the recorded data, by averaging the signal of adjacent OPD pixels with similar photocurrent output (at the expense of spatial resolution), eliminating signals that suffer from artefacts such as motion. The resulting high-quality PPG signal provides insight on the artery stiffness and the quality of blood circulation through a detailed analysis of the PPG second derivative, which has not been previously reported for organic oximeter arrays. The possibility of 2D oxygenation mapping capability combined with the high-quality PPG signals potentially provides substantial advantages in assessing tissue damaging or monitoring wounds, skin grafts, and organs.

We fabricated solution-processed NIR-sensitive OPDs based on poly[[2,5-bis(2-hexyldecyl)-2,3,5,6-tetrahydro-3,6-dioxopyrrolo[3,4-*c*]pyrrole-1,4-diyl]-*alt*-[2,2′:5′,2″-terthiophene]-5,5″-diyl] (PDPP3T), blended with phenyl-C$_{61}$-butyric acid methyl ester (PC$_{61}$BM). The chemical structures are displayed in **Figure 1**a. We used an inverted polarity OPD configuration where molybdenum oxide (MoO$_x$) and amorphous indium gallium zinc oxide (a-IGZO)

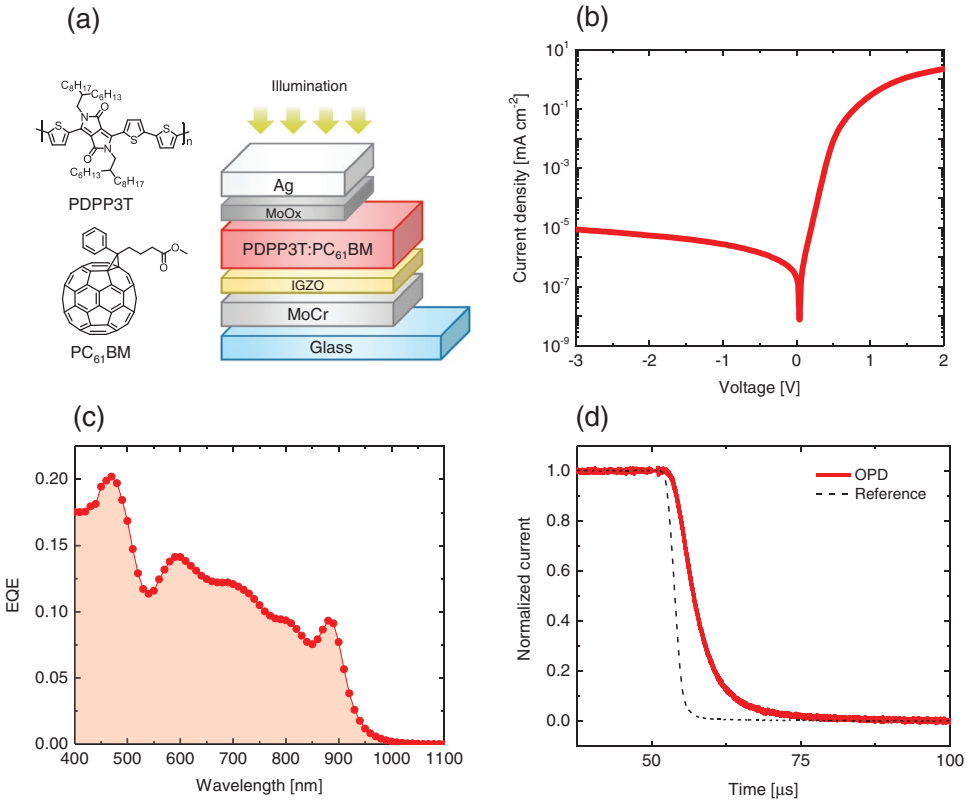

Figure 1. OPD materials and performance. a) Chemical structure of the donor polymer (PDPP3T) and the fullerene derivative acceptor (PC$_{61}$BM), and schematic of the OPD architecture. b) J–V characteristic in dark conditions. c) EQE spectrum at $V = -3$ V. d) Normalized photocurrent decay upon 730 nm light pulses of 50 µs duration. Fall time t_f, that is, time for response decrease from 90% to 10%, is 9.5 µs. The response of a Si-PD (dotted line) with the same active area is given for comparison.

were used as hole and electron extracting contacts under reverse bias, respectively. The OPDs were finished with a semi-transparent Ag (10 nm) top electrode.

The current density–voltage (J–V) characteristic recorded in dark conditions is shown in Figure 1b. The reverse bias dark current density (J_d) at $V = -3$ V is 8.5×10^{-6} mA cm^{-2}. While state-of-the-art J_d for green-sensitive OPDs based on wide band gap polymers ($E_0 \approx 2.0$ eV) ranges around 10^{-7} mA cm^{-2},[18–20] NIR-sensitive OPDs typically exhibit higher dark current densities.[21,22] This is mainly due to their smaller effective band gap (E_g), that is, the energy difference between the lowest unoccupied molecular orbital (LUMO) of the acceptor and the highest occupied molecular orbital (HOMO) of the donor, which enhances the probability of charge injection and/or bulk thermal generation in the active layer.[23] Indeed, the $PC_{61}BM$ LUMO and PDPP3T HOMO energies are −3.84 and −4.87 eV,[24] respectively, resulting in a rather low E_g of 1.03 eV. Nevertheless, the low J_d in the order of 10^{-6} mA cm^{-2} of our OPD is attributed to the charge blocking properties of a-IGZO, reducing the injection of holes under reverse bias.[25,26] This J_d value is comparable to previously reported dark current densities for organic pulse oximeters.[8,9] Regarding the OPD stability, the J–V characteristics show no visible signs of degradation after 2 weeks. In fact, previously reported OPDs based on the same architecture were demonstrated to show no signs of degradation after more than 1 year.[26]

Figure 1c shows the EQE spectrum with NIR sensitivity up to ≈950 nm. The EQE reaches ≈0.1 at the maximum of the first allowed optical absorption band of the polymeric semiconductor (≈900 nm). For OPD pixels in reflectance oximeter arrays, EQE >0.35 was previously reported.[9] The lower EQE of our OPDs is mainly due to the absorption of NIR radiation by the 10 nm Ag top electrode, resulting in a lower light intensity in the active layer. Substantial increase of the EQE in the NIR region can be achieved by replacing Ag with a transparent ITO top electrode, leading to EQE above 0.3 at 900 nm (Figure S1, Supporting Information). Despite the relatively low values, the EQE spectrum covers a wide wavelength range, from 400 to 950 nm. This broad spectral response is beneficial for PPG and SpO_2 applications.[27,28] Green wavelengths probe dermal arterioles, that is, the smaller-diameter blood vessels in the microcirculation that extends and branches out from an artery and leads to capillaries. With higher wavelengths, it becomes possible to probe deeper subcutaneous blood volume variations. Notably, green light has been shown to have the least influence from motion artifacts compared to red and NIR light PPG.[27] Pulse oximetry requires two distinct wavelengths and can be performed using green and red or red and NIR light, where the deeper penetration depth of NIR light was suggested to improve the invariance of SpO_2 measurements to skin non-homogeneities.[28]

In addition, we investigated the OPD time response by measuring photocurrent transients upon pulsed 730 nm illumination. We applied 50 µs pulses and recorded the decay in photocurrent upon the application of a light pulse, as shown in Figure 1d. The response of a Si photodiode is given for comparison. For these measurements, a circular aperture of 0.75 mm in radius defined the active area of both photodiodes. The OPD fall time t_f, that is, the time for response decrease from 90% to 10%, is 9.5 µs under a 16.1 mW cm^{-2} pulsed illumination. In this work, the PPG signals are obtained by sequentially measuring the signal at each wavelength: green (515 nm), red (630 nm), and near-infrared (850 and 940 nm). The measurements are performed using light and dark periods of 85 µs. The OPD response time ($t_f = 9.5$ µs) is nearly one orders of magnitude lower than the sampling time, indicating that the OPD is sufficiently fast for this application. The rise time is $t_r = 8$ µs (Figure S2, Supporting Information).

The 16 × 16 OPD array layout and operation are presented in **Figure 2**. The 256 pixels are arranged in a squared array with Y and X coordinates, as shown in Figure 2a. Each pixel is a square with a 0.9 mm side. The bottom electrodes of each pixel define the active areas, while the top electrode is common to all pixels. The pixel rows are spaced by 0.24 mm, while the columns are spaced by 0.5 mm to enable patterning of the conductive tracks. All metal interconnections are realized in the bottom layer. The yellow strip above the array is the area where the readout integrated circuit (ROIC) is placed to electrically connect each pixel individually (Figure S3, Supporting Information).

To achieve accurate PPG imaging using the 16 × 16 OPD array, two main prerequisites must be considered, namely the linearity of the photoresponse in each pixel, to ensure sensitive detection of small changes in light intensity, and the uniformity of the photoresponse over the whole pixel array, with negligible pixel-to-pixel photocurrent variations under the same lighting conditions. Both prerequisites are fulfilled by the 16 × 16 OPD array, as shown in Figure 2b. The red line indicates the mean photocurrent values over the 256 pixels at $V = -3$ V upon white OLED illumination. The photocurrent scales linearly with light intensity over the entire relevant range for application. The standard deviation (shaded area) is limited to ≈ 10% of the average values, which indicates a uniform photoresponse of the OPD array. In addition, the current density uniformity at $V = -3$ V under 90 cd cm^{-2} white OLED illumination and in dark conditions is illustrated in Figure 2c,e, respectively. The distribution of photocurrent under illumination can be fitted with a Gaussian curve having a narrow full width at half maximum (FWHM) of 1.6×10^{-3} mA cm^{-2} (Figure 2d). In most pixels, J_d in the order of 10^{-6} mA cm^{-2} is measured. Higher J_d values (around 10^{-4} mA cm^{-2}) are also obtained (Figure 2f). Although having a low dark current is, in general, beneficial for PPG application, we show that variations in J_d do not affect the quality of the final PPG signal as the array is operated at ambient light conditions.

We integrated the 16 × 16 OPD array into the experimental setup for PPG signal acquisition (**Figure 3**a). An LED array including green (515 nm), red (630 nm), and two different near-infrared (850 and 940 nm) wavelengths is used to illuminate the OPD array uniformly. The LED light travels through the spacing between the OPD pixels in the PPG array, reaches the finger, and is then reflected. As an opaque bottom electrode is used, only reflected light is detected by the OPD pixels. Taking into account the absorption of the other OPD layers, most notably the organic photoactive blend for some of the wavelengths used, we estimate that the optical flux density on the fingertip is decreased to 25% of the initial value (for the IR wavelength of 940 nm) and to 8% (for 850 nm). Figure 3b illustrates the current density distribution over the array in contact

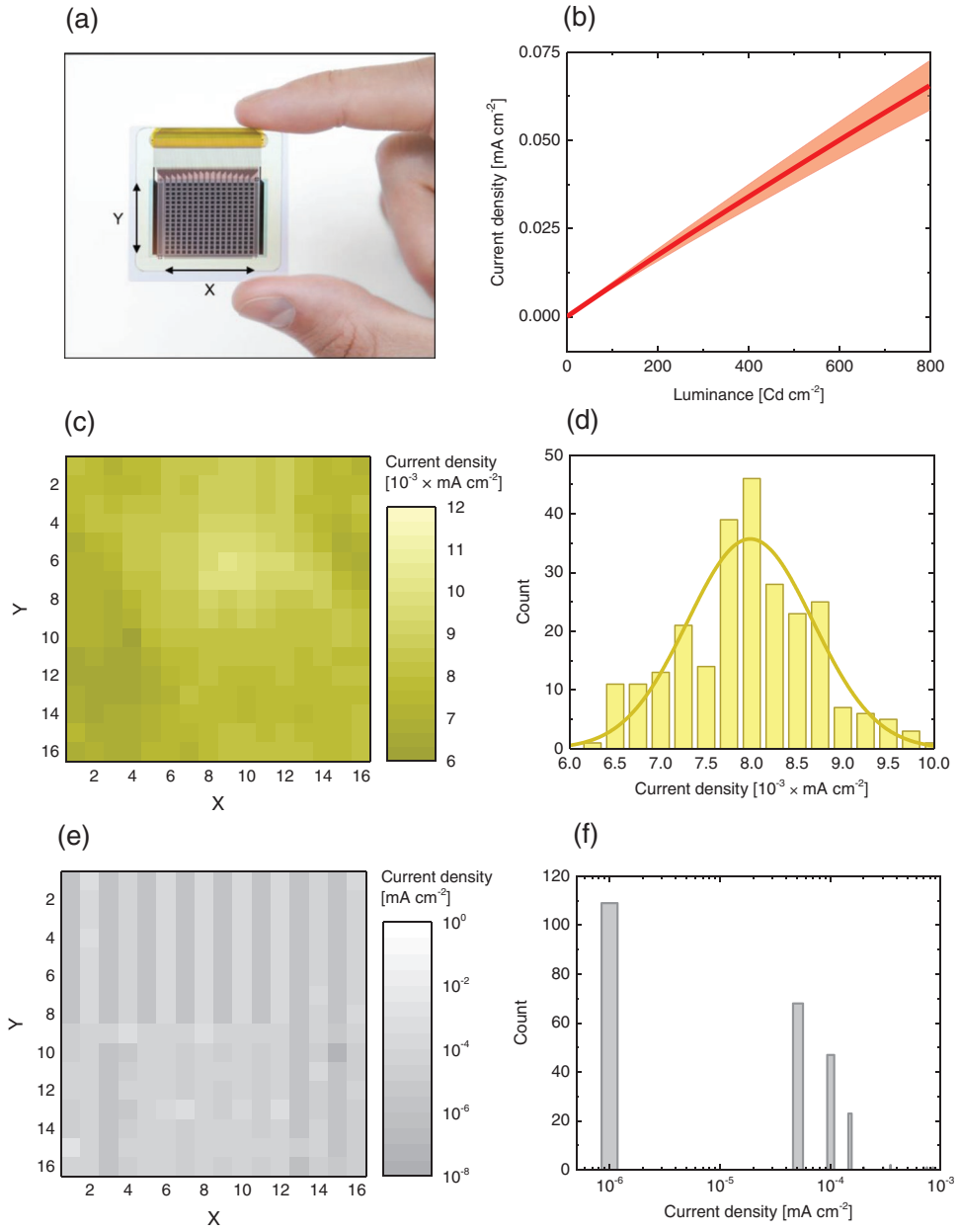

Figure 2. Operation of 16 × 16 OPD array. a) Photograph of OPD array. b) Linearity of photocurrent as function of light intensity for the 256 pixels upon white OLED illumination. The red line indicates the mean photocurrent values; the shaded area represents the standard deviation. Uniformity of the pixel array under c) 90 cd cm^{-2} illumination and e) in dark conditions. *X* and *Y* coordinates are defined as in (a). Current density distribution for the 256 pixels under d) 90 cd cm^{-2} illumination and f) in dark conditions.

with the finger. Higher photocurrent values are reached within the area where light is reflected by the fingertip, as approximately indicated by the white dashed line.

PPG imaging can potentially be achieved by recording the signal of each pixel in the 16 × 16 OPD array, thereby creating a 2D mapping of the PPG. Alternatively, the signal of adjacent pixels with similar photocurrent output can be averaged to increase the quality of the PPG. Since no substantial changes in the oxygenation level are expected over the area of the fingertip, we deliberately use pixel averaging as a (post-recording) strategy to improve the quality of the measurement rather than measuring oxygenation over the entire sensor area. Thus, this averaging operation enables to gain accuracy at the expense of the resolution. We can typically choose to average the PPG signals of pixels that exhibit variations in photoresponse of less than 10%, eliminating signals that seem corrupted by, for instance, motion artefacts. As an example, four pixels with such photoresponse variation are labeled with numbers 1–4 in Figure 3b. First, the PPG waveforms of each pixel (Figure S4, Supporting Information) are filtered by using a band-pass digital finite impulse response (FIR) filter from 0.5 to 10 Hz. The filtered signals of pixels 1–4 show negligible variations, as

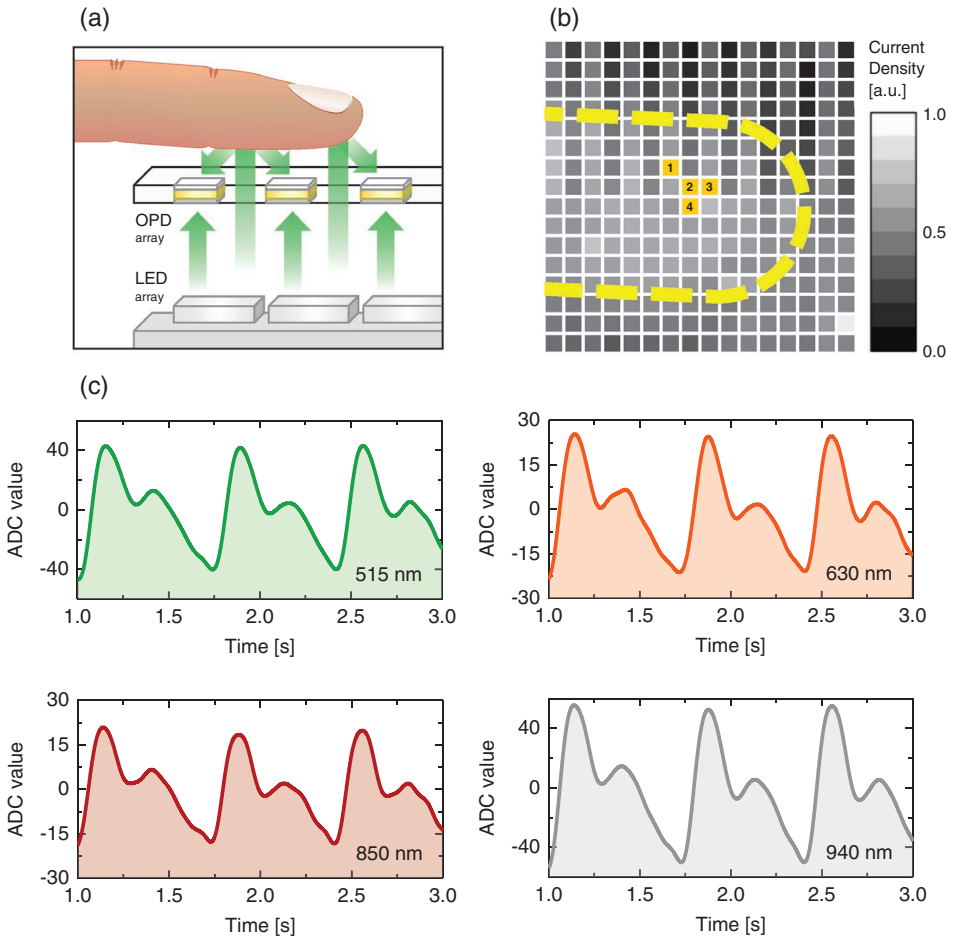

Figure 3. PPG signal acquisition using 16 × 16 OPD array. a) Schematic representation of the experimental setup for PPG signal acquisition. b) Current density distribution in the OPD array upon contact with the fingertip. Measured pixels are indicated with numbers 1–4. c) PPG signal acquired using LED illumination at different wavelengths. Full lines indicate the average signal among the four measured pixels.

shown in Figure S5, Supporting Information. Second, the individual waveforms are averaged. Figure 3c shows the resulting PPG signals at various wavelengths. Pixel averaging effectively leads to higher quality of the PPG waveforms by smoothening the features that might generate from movement or measurement artifacts during individual acquisitions (Figure S6, Supporting Information). PPG signals measured over a longer timescale (Figure S7, Supporting Information) show average variation in the main peak height as low as 5%, illustrating that the PPG signal is relatively stable over time.

Valuable information can be derived from the obtained PPG waveforms. State-of-the-art PPG signals are typically characterized by a rising edge (anacrotic phase) and a falling edge (catacrotic phase) of the pulse, related to the systole and diastole, respectively. A dicrotic notch generally appears in the catacrotic phase of individuals with healthy compliant arteries.[29] The location of systolic and diastolic peaks can be accurately determined from the zeroes of the PPG first derivative, as shown in **Figure 4** for the case of 515 nm LED illumination. Here, the PPG signal is recorded from a 34-year-old male volunteer. From the average systolic peak-to-peak interval a pulse rate of 86.7 beats per minute (bpm) is measured, which is within the normal resting rate range for individuals over the age of 10 years (60–100 bpm). The time delay ΔT between the systolic and diastolic peaks is related to the transit time of pressure waves from the root of the subclavian artery to the sensing location.[29] Assuming the path length to be proportional to subject height (h), a large artery stiffness index SI = $\Delta T/h$ of 6.6 is obtained, which lies within the typical range for adults (29–45 years of age). The value of ΔT (hence SI) decreases with age due to the enhanced artery stiffness and the higher pulse wave velocity in the aorta and large arteries.[29] We note that the finger PPG might be used to estimate the pulse arrival time (PAT) from the time delay between the electrocardiogram (ECG) R-peak and the maximum of the PPG waveform.[30,31] Typically, PATs in the order of hundreds of milliseconds are measured with this method,[31] indicating that the pulse arrival time is much shorter that the average peak-to-peak interval in the PPG signal.

Further insight on the blood circulation can be established from the second derivative of the PPG, also referred to as acceleration plethysmogram (APG).[32] The APG waveform typically includes four systolic waves (a–d) and one diastolic wave (e). These features are well visible in our APG. The location and height of each wave in the calculated APG waveform indicates proper blood circulation, as typically observed for healthy

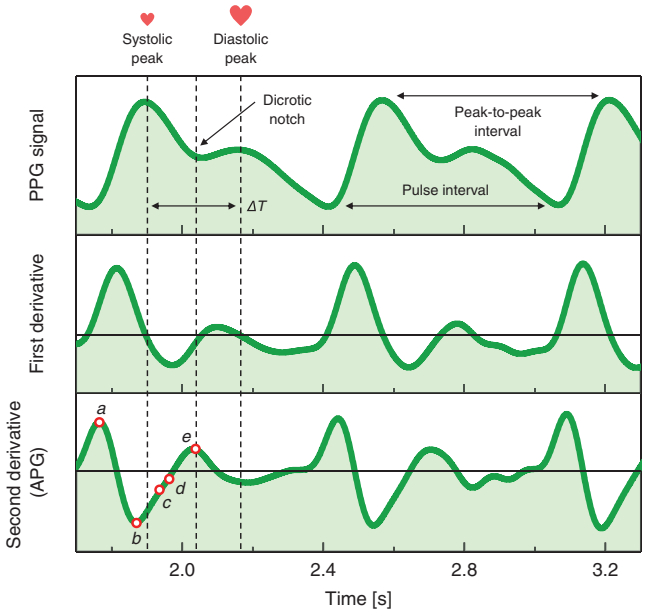

Figure 4. Analysis of PPG signal upon 515 nm LED illumination. The systolic and diastolic peaks can be accurately recognized from the analysis of the first derivative of the PPG signal. The location and height of each wave in the calculated acceleration plethysmogram (APG) waveform indicates proper blood circulation.

young people.[29] Notably, the b/a index (i.e., the height ratio of a and b waves) is considered to be the most promising index in the assessment of arterial health. We measured an average b/a index of –0.9. This falls into the experimental range for 34-year-old healthy volunteers, in contrast to diabetes patients for which $b/a > -0.4$ is found.[33]

Pulse oximeters can estimate blood oxygen saturation by optically quantifying the concentration of oxyhemoglobin (HbO_2) and deoxyhemoglobin (Hb). Interestingly, the molar extinction coefficients of HbO_2 (ε_{HbO_2}) and Hb (ε_{Hb}) vary considerably with wavelength, being the ratio $\varepsilon_{Hb}/\varepsilon_{HbO_2} < 2$, $\varepsilon_{Hb}/\varepsilon_{HbO_2} > 6$, and $\varepsilon_{Hb}/\varepsilon_{HbO_2} < 3$ in the green, red, and NIR region, respectively.[9] Therefore, the concentration of HbO_2 and Hb is typically measured combining red and green or red and NIR light to exploit the difference in molar extinction coefficient. The SpO_2 is given by the ratio between the concentration C of oxyhemoglobin and the total concentration of hemoglobin: $SpO_2 = \frac{C_{HbO_2}}{C_{HbO_2} + C_{Hb}}$.

In presence of a pulsatile PPG signal, oxygen saturation in reflection-mode oximetry (SpO_2^r) is assessed by modeling light propagation in the tissue via a modified Beer–Lambert's law in addition to an empirical correction, resulting in the following equation:[34]

$$SpO_2^r = \frac{\varepsilon_{Hb}(\lambda_1)\,DPF_{1-2} - \varepsilon_{Hb}(\lambda_2)\,R}{\left[\varepsilon_{Hb}(\lambda_1) - \varepsilon_{HbO_2}(\lambda_1)\right]DPF_{1-2} + \left[\varepsilon_{Hb}(\lambda_2) - \varepsilon_{HbO_2}(\lambda_2)\right]R} \quad (1)$$

The complete derivation of Equation (1) is provided in ref. [9]. Here, $\varepsilon_{Hb}(\lambda)$ and $\varepsilon_{HbO_2}(\lambda)$ are the molar extinction coefficients of oxyhemoglobin and deoxyhemoglobin at wavelength λ, while the subscripts 1 and 2 indicate the red (630 nm) and infrared (850 or 940 nm) wavelengths, respectively. DPF_{1-2} is the differential pathlength factor accounting for multiple light scattering within the tissue, and R is the ratio of pulsatile (AC) to stationary (DC) signals at the two wavelengths, given by $R = \frac{AC_1/DC_1}{AC_2/DC_2}$. To estimate SpO_2^r, we measured R using a combination of 630–850 or 630–940 nm LED lights. SpO_2^r decreases with increasing R as predicted by the Beer–Lambert's model[35] (Figure S8, Supporting Information). For instance, at SpO_2 level of 99%, R is equal to 0.51 and 0.59 for 630–850 and 630–940 nm illumination, respectively. To obtain agreement with transmission-mode oximetry (SpO_2^t) data measured with a commercial finger probe at SpO_2 level of 99% using the aforementioned R values, we found $DPF_{630-850\ nm} = 0.82$ and $DPF_{630-940\ nm} = 1.1$. Indeed, DPF_{1-2} values in the order of unity have been previously reported at these wavelengths.[36,37] Therefore, the correct SpO_2 level can be estimated using experimentally determined R values and assuming state-of-the-art DPF values in the order of unity.

In summary, we developed a 16 × 16 OPD pixel array and we demonstrated its potential for PPG measurements and pulse oximetry. The discrete OPD pixels show spectral sensitivity over the visible and NIR spectrum up to 900 nm. The photogenerated current in each pixel scales linearly with light intensity across the range used in this work, and the photoresponse is uniform over the entire pixel array. Our OPD array can potentially map the PPG signal over a large area with higher resolution compared to previously reported works. In addition, the pixelated nature of the array allows further improvement of the PPG signal quality improved further in a post-processing stap by averaging the signal of adjacent OPD pixels with similar photocurrent output. The resulting high-quality PPG signals enabled to gain insights on the artery stiffness and the quality of blood circulation. Finally, oxygen saturation can be assessed correctly by using experimentally determined R values and by assuming differential pathway factors in the order of unity, in agreement with previously reported DPF values. Our OPD array potentially enables a smart bandage that has high-resolution oxygenation mapping capability, which may find clinical value in skin health assessments monitoring wounds, skin grafts, and organs.

Experimental Section

OPD Fabrication: The discrete OPDs and the 16 × 16 OPD array were made using with the same fabrication method. A 130 nm chromium molybdenum alloy (MoCr) film was sputtered on glass and subsequently patterned with photolithography to form the bottom electrode. Next, a thin film (32 nm) of a-IGZO was sputtered on the bottom electrode. PDPP3T (CalOS) was blended with $PC_{61}BM$ (nano-c) 1:2 w/w in a chloroform solution with 7.5 vol% o-dichlorobenzene at 7 mg mL^{-1} polymer concentration. The PDPP3T:$PC_{61}BM$ blend was cast by spin coating at 750 rpm in a N_2-filled glovebox resulting in a ≈ 280 nm layer. The processing conditions to deposit the BHJ layer have been previously optimized to achieve optimal phase separation and morphology in terms of device photoresponse.[38] The active layer was dried overnight in a vacuum chamber at ≈6 × 10^{-7} mbar. The top electrode consisted of evaporated MoO_x (60 nm) and Ag (10 nm) (both purchased at Alfa Aesar). The active area of the discrete OPDs was 2 × 2 mm. In the 16 × 16 OPD array, a flexible thin film was used to provide the electrical connection between each pixel and the ROIC.

Discrete OPD Characterization: *J–V* characteristics in dark conditions were measured with a probe station in a N_2-filled glovebox. The voltage

was swept from −3 V to +2 V and back. Displacement currents were minimized using a slow scan speed of 0.05 V s^{-1}. The EQE setup consisted of a tungsten–halogen lamp, a chopper, a monochromator (Oriel, Cornerstone 130), a pre-amplifier (Stanford Research Systems SR570), and a lock-in amplifier (Stanford Research Systems SR830 DSP). The photocurrent transients were acquired by pulsing the NIR LED light with a waveform generator (Agilent 33250A) and recording the current as function of time with an oscilloscope (Tektronix TDS5052B). A circular aperture of 0.75 mm in radius defined the active area for the EQE and photocurrent transient measurements.

16 × *16 OPD Array Characterization*: Photocurrent measurements as function of light intensity were performed illuminating the 16 × 16 OPD array with a white OLED tile. The OLED emission spectrum is shown in Figure S9, Supporting Information. The OLED tile was driven using a voltage source (TTi EL302R Power Supply). PPG signals were acquired using an array of LEDs of four different wavelengths: 515, 630, 850 and 940 nm (Würth Elektronik, 150141GS73100, 150141RS73100, 15414185BA210, and 15414185BA210, respectively). Four LEDs were used per wavelength. In both cases, the OPD response was measured using a custom-made electronic system and software (LabVIEW based). A silicon readout IC (Analog Device AD71124) collects all the 256 pixels. The chip is biased at −1 V using a custom-made board and connected to an FPGA digital interface that reads the data. The FPGA interface is connected to a PC through a USB.

Supporting Information

Supporting Information is available from the Wiley Online Library or from the author.

Conflict of Interest

The authors declare no conflict of interest.

Keywords

bulk heterojunction, heartbeat, organic photodiodes, photoplethysmography, pulse oximetry

Received: November 27, 2019
Revised: February 7, 2020
Published online: March 16, 2020

[1] J. Allen, *Physiol. Meas.* **2007**, *28*, R1.
[2] P. Leonard, T. F. Beattie, P. S. Addison, J. N. Watson, *Emerg. Med. J.* **2003**, *20*, 524.
[3] P. S. Addison, J. N. Watson, M. L. Mestek, J. P. Ochs, A. A. Uribe, S. D. Bergese, *J. Clin. Monit. Comput.* **2015**, *29*, 113.
[4] A. Krishnamohan, V. Siriwardana, J. J. Skowno, *Pediatr. Anesth.* **2016**, *26*, 1106.
[5] S. Seifi, A. Khatony, G. Moradi, A. Abdi, F. Najafi, *BMC Nurs.* **2018**, *17*, 15.
[6] A. N. Nicolaides, C. Miles, *J. Vascul. Surg.* **1987**, *5*, 405.
[7] H. Lee, H. Ko, J. Lee, *ICT Express* **2016**, *2*, 195.
[8] C. M. Lochner, Y. Khan, A. Pierre, A. C. Arias, *Nat. Commun.* **2014**, *5*, 5745.
[9] Y. Khan, D. Han, A. Pierre, J. Ting, X. Wang, C. M. Lochner, G. Bovo, N. Yaacobi-Gross, C. Newsome, R. Wilson, A. C. Arias, *Proc. Natl. Acad. Sci. USA* **2018**, *115*, E11015.
[10] T. Yokota, P. Zalar, M. Kaltenbrunner, H. Jinno, N. Matsuhisa, H. Kitanosako, Y. Tachibana, W. Yukita, M. Koizumi, T. Someya, *Sci. Adv.* **2016**, *2*, e1501856.
[11] H. Lee, E. Kim, Y. Lee, H. Kim, J. Lee, M. Kim, H. Yoo, S. Yoo, *Sci. Adv.* **2018**, *4*, eaas9530.
[12] R. D. Jansen-van Vuuren, A. Armin, A. K. Pandey, P. L. Burn, P. Meredith, *Adv. Mater.* **2016**, *28*, 4766.
[13] I. Deckman, P. B. Lechêne, A. Pierre, A. C. Arias, *Org. Electron.* **2018**, *56*, 139.
[14] G. Williams, C. Backhouse, H. Aziz, *Electronics* **2014**, *3*, 43.
[15] S. Choi, H Lee, R. Ghaffari, T. Hyeon, D. Kim, *Adv. Mater.* **2016**, *28*, 4203.
[16] T. Q. Trung, N. Lee, *Adv. Mater.* **2016**, *28*, 4338.
[17] T. Yokota, T. Nakamura, H. Kato, M. Mochizuki, M. Tada, M. Uchida, S. Lee, M. Koizumi, W. Yukita, A. Takimoto, T. Someya, *Nat. Electron.* **2020**, *3*, 113.
[18] G. H. Gelinck, A. Kumar, D. Moet, J. P. J. Van Der Steen, A. J. J. M. Van Breemen, S. Shanmugam, A. Langen, J. Gilot, P. Groen, R. Andriessen, M. Simon, W. Ruetten, A. U. Douglas, R. Raaijmakers, P. E. Malinowski, K. Myny, *IEEE Trans. Electron Devices* **2016**, *63*, 197.
[19] A. Pierre, I. Deckman, P. B. Lechêne, A. C. Arias, *Adv. Mater.* **2015**, *27*, 6411.
[20] M. Biele, C. Montenegro Benavides, J. Hürdler, S. F. Tedde, C. J. Brabec, O. Schmidt, *Adv. Mater. Technol.* **2019**, *4*, 1800158.
[21] M. Binda, A. Iacchetti, D. Natali, L. Beverina, M. Sassi, M. Sampietro, *Appl. Phys. Lett.* **2011**, *98*, 073303.
[22] X. Zhou, D. Yang, D. Ma, *Adv. Opt. Mater.* **2015**, *3*, 1570.
[23] K. Baeg, M. Binda, D. Natali, M. Caironi, Y. Noh, *Adv. Mater.* **2013**, *25*, 4267.
[24] R. E. M. Willems, L. C. H. Weijtens, X. de Vries, R. Coehoorn, R. A. J. Janssen, *Adv. Energy Mater.* **2019**, *9*, 1803677.
[25] H. Arora, P. E. Malinowski, A. Chasin, D. Cheyns, S. Steudel, S. Schols, P. Heremans, *Appl. Phys. Lett.* **2015**, *106*, 143301.
[26] D. Tordera, B. Peeters, H. B. Akkerman, A. J. J. M. van Breemen, J. Maas, S. Shanmugam, A. J. Kronemeijer, G. H. Gelinck, *Adv. Mater. Technol.* **2019**, *4*, 1900651.
[27] Y. Maeda, M. Sekine, T. Tamura, *J. Med. Syst.* **2011**, *35*, 969.
[28] A. V. Moço, S. Stuijk, G. de Haan, *Sci. Rep.* **2018**, *8*, 8501.
[29] M. Elgendi, *Curr. Cardiol. Rev.* **2012**, *8*, 14.
[30] S. Rajala, H. Lindholm, T. Taipalus, *Physiol. Meas.* **2018**, *39*, 075010.
[31] S. Rajala, T. Ahmaniemi, H. Lindholm, T. Taipalus, *Conf. Proc. IEEE Eng. Med. Biol. Soc.*, **2018**, *2018*, 5685.
[32] Y. K. Qawqzeh, R. Uldis, M. Alharbi, *Sci. Res. Essays* **2015**, *10*, 633.
[33] K. Pilt, K. Meigas, K. Temitski, M. Viigimaa, *IFMBE Proc.* **2012**, *39*, 410.
[34] J. G. Webster, *Design of Pulse Oximeters*, Institute of Physics, Bristol, UK **1997**.
[35] H. Cao, *Design of Wireless Physiological Measurement Systems for Patients Affected by COPD*, UQAC, Québec **2017**.
[36] F. Scholkmann, M. Wolf, *J. Biomed. Opt.* **2013**, *18*, 105004.
[37] A. Duncan, J. H. Meek, M. Clemence, C. E. Elwell, L. Tyszczuk, M. Cope, D. T. Delpy, *Phys. Med. Biol.* **1995**, *40*, 295.
[38] M. Li, J. Li, D. Di Carlo Rasi, F. J. M. Colberts, J. Wang, G. H. L. Heintges, B. Lin, W. Li, W. Ma, M. M. Wienk, R. A. J. Janssen, *Adv. Energy Mater.* **2018**, *8*, 1800550.